Liquid Crystals
Publication details, including instructions for authors and subscription information:
http://www.informaworld.com/smpp/title~content=t713926090

Impurities in nematic liquid crystal samples inducing changes in the DSM1-DSM2 transition phase diagram

D. E. Lucchetta; N. Scaramuzza; G. Strangi; C. Versace

Online publication date: 06 August 2010

To cite this Article Lucchetta, D. E. , Scaramuzza, N. , Strangi, G. and Versace, C.(2000) 'Impurities in nematic liquid crystal samples inducing changes in the DSM1-DSM2 transition phase diagram', Liquid Crystals, 27: 2, 277 — 281
To link to this Article: DOI: 10.1080/026782900203092
URL: http://dx.doi.org/10.1080/026782900203092

LIQUID CRYSTALS, 2000, VOL. 27, NO. 2, 277–281

Impurities in nematic liquid crystal samples inducing changes in the DSM1–DSM2 transition phase diagram

D. E. LUCCHETTA, N. SCARAMUZZA*, G. STRANGI and C. VERSACE

Dipartimento di Fisica dell'Università della Calabria and Istituto Nazionale per la Fisica della Materia, UdR della Calabria, I-87036 Rende, Cosenza, Italy

(*Received 18 June 1999; accepted 31 August 1999*)

In this paper we report, for the first time, the experimental phase diagram for the DSM1–DSM2 transition. We show the effects due to changes in the conductivity anisotropy resulting from impurities introduced in the cases of both homeotropic and homogeneously planar aligned nematic liquid crystal cells.

1. Introduction

Recently, the transition among turbulent states driven by an external voltage has also been observed after a sequence of electroconvective instabilities in homeotropically aligned nematic liquid crystal (NLC) samples [1, 2]. The phenomenon shows many points in common with the planar case, and the overlapping between the two turbulent regimes seems to be very similar. Moreover, in recent work [3] on the nucleation rate and the growth velocity of DSM2 turbulent nuclei, we have characterized the transition between the two turbulent regimes in a homeotropically aligned NLC.

Let us consider a NLC homogeneously planar aligned exhibiting negative dielectric anisotropy ($\Delta\varepsilon = \varepsilon_{\parallel} - \varepsilon_{\perp} < 0$, where $\varepsilon_{\parallel}$ and $\varepsilon_{\perp}$ are the dielectric constants parallel and perpendicular to the director, respectively) and positive conductivity anisotropy ($\Delta\sigma = \sigma_{\parallel} - \sigma_{\perp} > 0$, where $\sigma_{\parallel}$ and $\sigma_{\perp}$ are the conductivities parallel and perpendicular to the director, respectively). From a strictly phenomenological point of view, by application at a fixed frequency (less than the cut-off frequency, i.e. the relaxation frequency of the space charges in the liquid crystal [4]) of a voltage whose amplitude is gradually increased, it is possible to observe the following principal dynamic regimes [5]: the Williams–Kasputin domains, the weak turbulence, and the dynamic scattering modes (DSM1 and DSM2).

In a planar sample of the NLC MBBA (*N*-(*p*-methoxybenzilidene)-*p*-*n*-butylaniline), the first instability that appears above a threshold voltage V_w of about 6.8 V consists of a periodic pattern of convective rolls (the Williams–Kasputin domains). This instability arises as a result of the competition between a pure dielectric restoring force, resulting from the negative dielectric anisotropy, and a force exerted on the bulk fluid due to the charge separation produced by the positive conductive anisotropy [6]. Observing the NLC sample by polarizing microscopy, the periodic deformation appears like a series of alternating dark and bright domains that run perpendicular to the original alignment. The wavelength of the periodic deformation is determined by the thickness of the cell [7]. The domain lines are the result of light focused on different planes [8] by the periodic array of lenses due to the refractive index modulations induced by the a.c. voltage on increasing the driving voltage, the rolls undulate and reach a weak turbulent state.

Experimentally it is also observed that, when the applied voltage exceeds the threshold voltage V_w, the rotational velocity of the fluid increases [9]. The fluid gradually becomes more turbulent until a break in the molecular anchoring at the surface occurs, with the director tilting in a different direction with respect to the original undistorted orientation [10].

For this reason, at even higher values of the applied voltage, a change from the turbulent state DSM1 to the strong turbulent state DSM2 is observed. In order to obtain the transition between DSM1 and DSM2, it is only necessary to apply, at fixed frequency, a voltage $V > V_{th}$ (here V_{th} represents the threshold voltage value of DSM2 at that frequency) and to wait for a time interval which decreases drastically with high voltage values. The transition between the two turbulent regimes takes place through nucleation of small areas of DSM2 and their subsequent growth.

* Author for correspondence;
e-mail: scaramuzza@fis.unical.it

Liquid Crystals ISSN 0267-8292 print/ISSN 1366-5855 online © 2000 Taylor & Francis Ltd
http://www.tandf.co.uk/journals/tf/02678292.html

The intense light scattering caused by the DSM1 state is spatially anisotropic and probably this dynamic regime is characterized by the presence of small convective structures of the order of a few microns. On the contrary, the light scattering in the DSM2 state is spatially isotropic, and in this regime no structure can be observed [11]. Finally, it must be noted that the onset of the DSM2 is a nucleation process very similar to that observed in some non-convective systems such as classical crystal growth.

In the case of homeotropically aligned NLC samples, where the director aligns perpendicular to the glass plates, the situation is slightly different. In fact, above a certain voltage threshold, a well known molecular reorientation phenomenon occurs (Fréedericksz transition) [12]. At higher values of the applied voltage, still in the electro-hydrodynamic convection (EHC) condition, it is possible to observe a long series of structures constituted by extremely complex patterns that are also difficult to reproduce. In spite of this, even in this case it is easy to observe the transition between turbulent states. These two turbulent states are optically similar to DSM1 and DSM2 regimes found in the planar case; therefore, for simplicity, we use the same reference notation.

In this paper we deal mainly with the experimental determination of the threshold voltage for the DSM1–DSM2 transition for both planar and homeotropically aligned NLC cells. The study of the effects due to changes in the conductive anisotropy resulting from the introduction of impurities into the samples is considered a point of great interest for this new kind of turbulent decay.

2. Experimental results and discussion

The sample cell consisted of two parallel square ($30 \times 30\,mm^2$) glass plates spaced by two mylar strips ($d \cong 36\,\mu m$). Both surfaces of the glass plates were coated with indium tin oxide (ITO) tansparent electrodes. In order to obtain both the homeotropic and the planar alignment, the surfaces of the glass plates were treated by the following surfactants: *N*,*N*-dimethyl-*N*-octadecyl-*N*-[3-(trimethoxysilyl)propyl]ammonium chloride (DMOAP from Aldrich) and ACM72 (Atomergic Chemetals Corporation), successively.

In order to obtain different values of the conductivity, eleven different cells (six planar and five homeotropic) were filled with nematic MBBA, at different wt % values of the doping material with the molecular structure shown in figure 1.

The cell was mounted in a thermally insulated oven, the temperature of which was kept at 24°C by a HAAKE F3 water bath thermostat. An a.c. voltage was applied perpendicularly to the glass plates (*z*-direction).

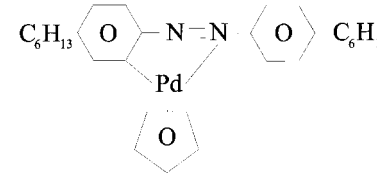

Figure 1. Structure of the doping agent.

Figure 2 shows the experimental geometry. A 2 mW linearly polarized He-Ne laser beam was split into two parts (the probe beam and the reference beam) by means of a semi-transparent mirror. The circularly polarized and intensity modulated probe beam hit the cell perpendicularly to its cover plate, the beam waist being 0.2 mm, so that the resulting spatial resolution of the volume of the laser beam was $45 \times 10^{-4}\,mm^3$. The intensity of the transmitted light was detected by a photodiode and the electric signal was phase measured by a Lock-in Analyser (EG&G Mod. 7260). The reference intensity, revealed by a second silicon photodiode (having the same characteristic as the first one) was sent to the ratio input of the Lock-in Analyser. This last signal was used to normalize instantaneously the response of the NLC sample and to prevent errors due to possible fluctuations of the laser beam intensity. An operational amplifier (KEPCO Mod. BOP1000) driven by a waveform generator (HP Mod. 33120A) supplied the external voltage to the sample. All the measurements were controlled by a personal computer, which provided the acquisition and storage of the data, the control of the oven temperature and the linear amplitude sweep for a user-defined range and rate. The frequency of the external applied voltage ranged from 30 to 600 Hz in

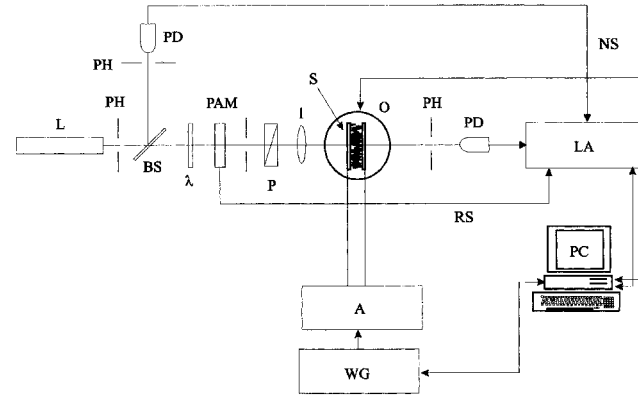

Figure 2. The experimental set-up. L: He-Ne laser, PH: pinhole, BS: beam splitter, PD: photodiode, P: polarizer, PAM: photo-acoustic modulator, l: lens, S: NLC sample, O: oven, A: amplifier, WG: waveform generator, LA: lock-in amplifier, PC: personal computer, λ: quarter wave retarder, NS: normalization signal, RS: reference signal.

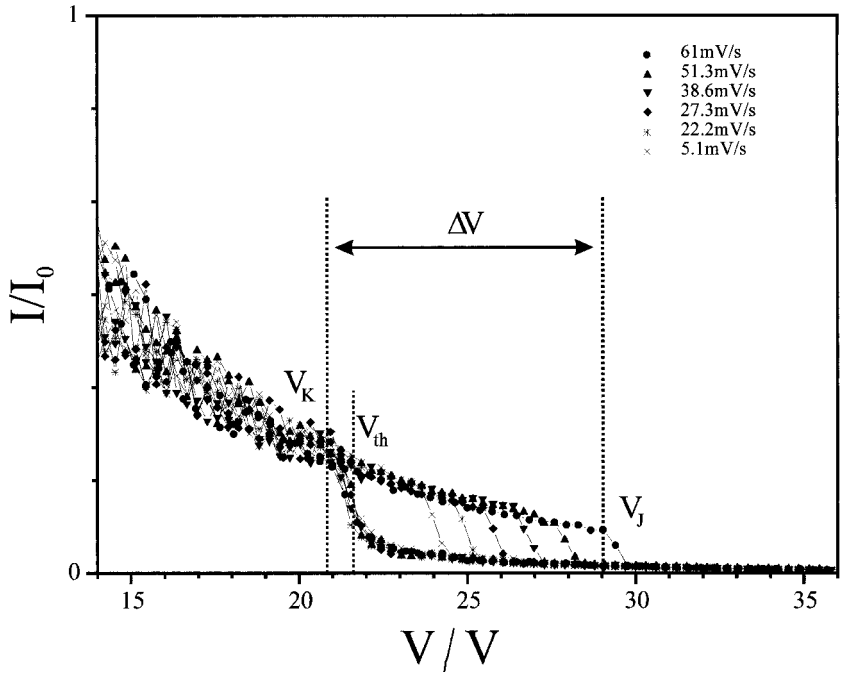

Figure 3. Hysteresis in light transmittance I/I_0, for a homeotropic sample with $\sigma_{\parallel} = 7.1 \times 10^{-10}\ \Omega^{-1}\,cm^{-1}$, near the DSM1–DSM2 transition for different ramp rates r ($mV\,s^{-1}$). The ramp values used range from 1 to 65 $mV\,s^{-1}$ at the fixed frequency of 200 Hz and $T = 24°C$.

the planar case and from 30 to about 1000 Hz in the homeotropic case. These values depend on the sample conductivity anisotropy $\Delta\sigma$ and were always below the measured cut-off frequency [13].

The conductivities $\sigma_{\parallel}$ and $\sigma_{\perp}$ of the samples were measured by using an impedance meter EGG Mod. 273A.

In order to verify the existence of a threshold voltage for the DSM1–DSM2 transition, the applied voltage V was swept in amplitude at different rates r ($mV\,s^{-1}$) in the neighbourhood of the DSM1–DSM2 transition. In figure 3 the voltage dependence of the light transmittance is shown as a function of the applied voltage. On increasing the voltage, the light transmittance exhibited a sudden change in slope at a voltage V_J that depends on the rate r; therefore we can consider it as an r-dependent DSM2 threshold. Above V_J the DSM2 nuclei rise and grow spontaneously and a greater and greater amount of light is scattered out from the transmitted beam (in the homeotropic cases we obviously did not observe the strong dependence on the polarization of the incident light found for the planar case). Unlike V_J, the voltage V_K that represents the DSM2–DSM1 threshold on decreasing the applied voltage is rather insensitive to changes in r. The difference $\Delta V = V_J - V_K$ tends to zero as r decreases. Obviously, because of this behaviour we can assume V_K to be the DSM2 threshold.

In figure 4 is shown the dynamic hysteresis behaviour for two different frequencies of the applied voltage. We

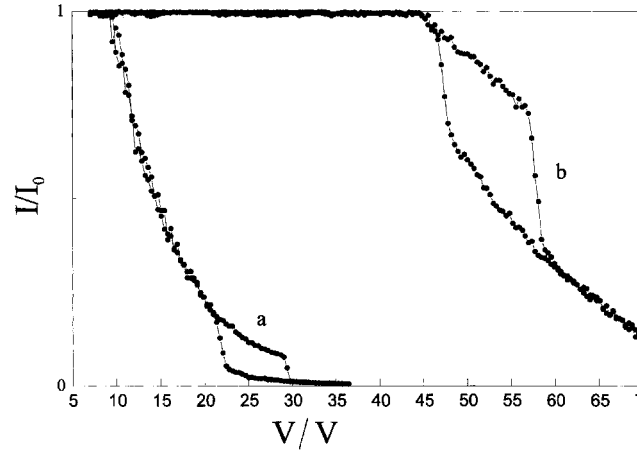

Figure 4. Dynamic hysteresis in light transmittance near the DSM1–DSM2 transition point; ramp rate $r = 50\ mV\,s^{-1}$. (*a*) $f = 234$ Hz, (*b*) $f = 518$ Hz at $T = 24°C$ and $\sigma_{\parallel} = 7.1 \times 10^{-10}\ \Omega^{-1}\,cm^{-1}$.

can observe that, at fixed ramp rate the hysteresis at high frequency values is obviously wider than that observed at low frequency values, as already observed for the planar case [14].

Let us define the external control parameter $\mathcal{E}_2$ for the transition:

$$\mathcal{E}_2 = \frac{(V_0^2 - V_{th}^2)}{V_{th}^2}.$$

In figure 5 is shown a series of images take at different times bearing evidence of the nucleation phenomenon for both planar and homeotropic samples of the NLC. In both cases the temperature was kept at 24°C, the frequency at 70 Hz, and the external applied voltage was suddenly increased from 0, whereupon, $\mathcal{E}_2$ increased to 2.1 (planar) and 10.7 (homeotropic).

The darkest regions are the spontaneously created DSM2 nuclei. With time the nuclei grow until they merge with other nuclei. Simultaneously, new nuclei are created in the remaining DSM1 area until the DSM2 state spreads all over the sample.

It is interesting to note that in the case of a planarly aligned sample, the DSM2 nuclei are always roughly elliptical in shape with the long axis parallel to the planar anchoring direction. On the other hand, in the case of the homeotropically aligned sample, the DSM2 nuclei display a clearly circular form. Moreover, the number of nucleation sites increases with increasing external applied voltage, as shown in figure 6.

Finally, in figures 7 and 8 the DSM2 threshold voltage behaviour with respect to the frequency of the external applied voltage and for different conductivity values is reported, for planar and homeotropic samples, respectively. It is worthwhile noting that in both the cases the dependence of the DSM2 threshold on the applied voltage frequency seems to obey an exponential growth law; that is, as the frequency reaches the conductive-dielectric regime cut-off frequency, the DSM2 drastically augments. Furthermore, at a fixed frequency, the threshold decreases as the dopant concentration, i.e. the conductivity of the sample, increases.

According to [15] this behaviour can be ascribed to the absorption of ionic impurities at the surfaces that decrease the NLC–substrate anchoring energy. These considerations confirm the interpretation of the DSM1–DSM2 transition in terms of anchoring breaking, as suggested in our previous paper [11]. Moreover, we observe that the threshold is lower in the homeotropically aligned sample, and it is well known that generally homeotropic anchoring energy is lower than that for planar anchoring.

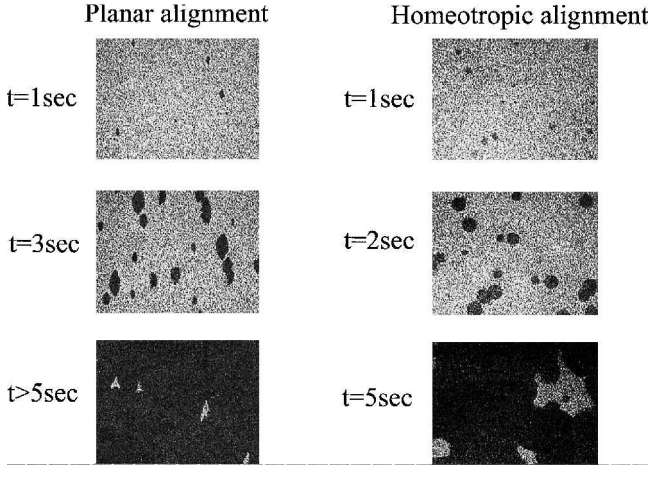

Figure 5. A set of photographs of the growth process of DSM2 nuclei at different times after applying a voltage V larger than the DSM2 threshold voltage V_{th} (see the text).

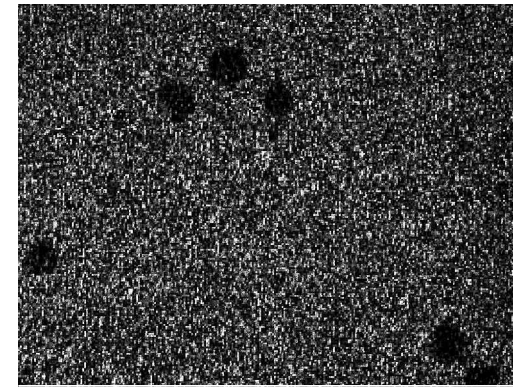

(*a*)

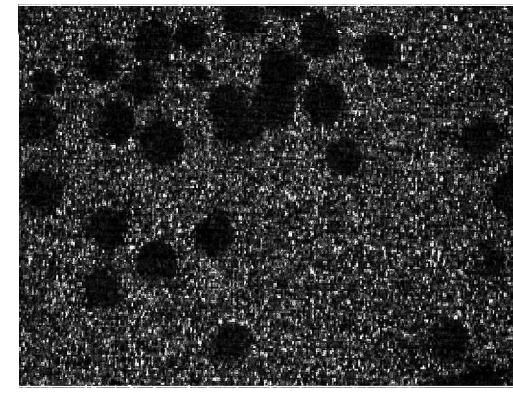

(*b*)

Figure 6. Number of nucleation sites at $V = 35$ V (*a*) and $V = 60$ V (*b*) about 4 s after applying the voltage at $f = 70$ Hz, $T = 24$°C and $\sigma_{\parallel} = 9 \times 10^{-10}\ \Omega^{-1}\,\mathrm{cm}^{-1}$, for a homeotropic sample 36 μm thick.

3. Conclusions

In this work we have studied how the threshold voltage of the DSM2 regime depends on the conductivity of the NLC, in the case of both planar and homeotropically aligned samples. In both cases the introduction of impurities into the cells produced an increase in the values of the conductivity. There is also a notable shift of the cut-off frequencies. If we go beyond these values, it is not possible to observe the DSM1–DSM2 transition.

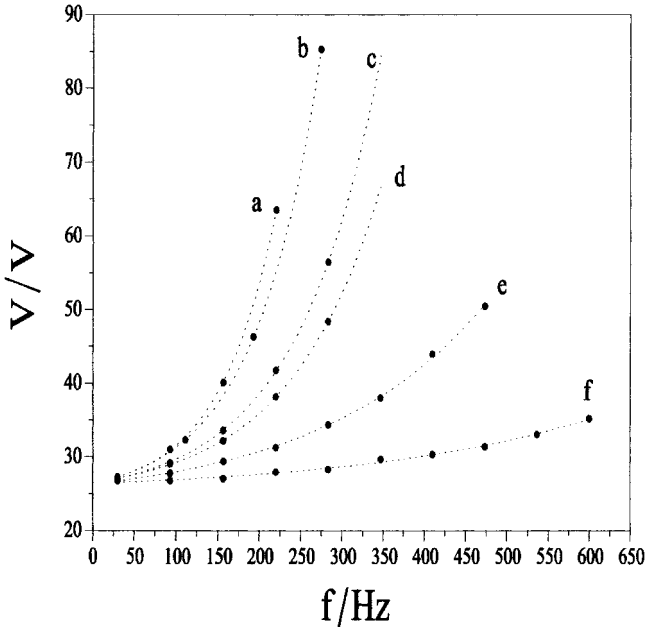

Figure 7. Behaviour of the DSM2 threshold voltage with respect to the frequency for a planar NLC sample at $T = 24°C$. $\sigma_{\perp} = (a)\ 1.95 \times 10^{-10}$, $(b)\ 2.13 \times 10^{-10}$, $(c)\ 2.61 \times 10^{-10}$, $(d)\ 3.04 \times 10^{-10}$, $(e)\ 6.2 \times 10^{-10}$, $(f)\ 1.2 \times 10^{-9}\ \Omega^{-1}\,cm^{-1}$.

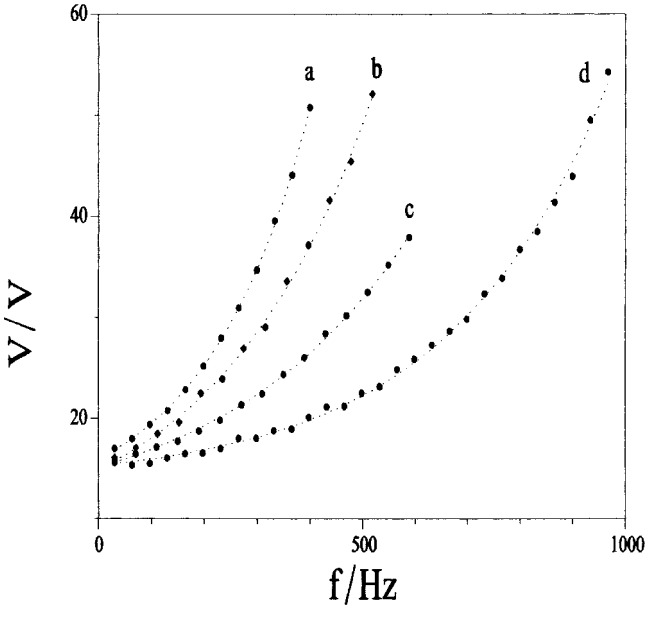

Figure 8. Behaviour of the DSM2 threshold voltage with respect to the frequency for a homeotropic NLC sample at $T = 24°C$. $\sigma_{\parallel} = (a)\ 5.7 \times 10^{-10}$, $(b)\ 7.1 \times 10^{-10}$, $(c)\ 9 \times 10^{-10}$, $(d)\ 3.4 \times 10^{-9}\ \Omega\,cm^{-1}$.

Using the same percentage of impurities, the DSM2 threshold voltage is lower in the homeotropic case than in the planar case. Thus the nucleation process is made easy in the homeotropic samples, whereas for the same external applied voltage the minimum area for one nucleation phenomenon is about the same [3].

Our measurements validate the interpretation of the DSM1–DSM2 transition in terms of an anchoring breaking.

In conclusion, we think that a better understanding of the EHC and in particular of the nucleation phenomenon that takes place at the DSM1–DSM2 transition could be useful to gain insight into the problem of anchoring breakage, which is of interest for novel LCD technology.

The authors are indebted to R. Bartolino for fruitful discussions and helpful suggestions. The authors would like to thank B. De Nardo and C. Prete for their technical aid.

References

[1] Kai, S., Hayashi, K., and Hidaka, Y., 1996, *J. phys. Chem.*, **100,** 19 016.
[2] Fazio, S. U., Komitov, L., and Lagerwall, S. T., 1998, in Proceedings of the 17th International Conference on Liquid Crystals, Strasbourg, France, P3–79.
[3] Lucchetta, D. E., Scaramuzza, N., Strangi, G., and Versace, C., 1999, *Phys. Rev. E* (in the press).
[4] Dubois-Violette, E., de Gennes, P. G., and Parodi, O., 1971, *J. Physique*, **32,** 35.
[5] Kai, S., and Zimmermann, W., 1989, *Progr. theor. Phys. Suppl.*, **99,** 458.
[6] Carr, E. F., 1963, *J. chem. Phys.*, **39,** 1979; Helfrich, W., 1969, *J. chem. Phys.*, **51,** 4092.
[7] Williams, R., 1963, *J. chem. Phys.*, **39,** 384.
[8] Joets, A., and Ribotta, R., 1986, *J. Physique*, **47,** 595; Joets, A., and Ribotta, R., 1994, *J. Physique* I, **4,** 1013.
[9] Carrol, T. O., 1972, *J. appl. Phys.*, **43,** 1342.
[10] Scaramuzza, N., Versace, C., and Carbone, V., 1995, *Mol. Cryst. liq. Cryst.*, **266,** 85.
[11] Carbone, V., Scaramuzza, N., and Versace, C., 1997, *Physica D*, **106,** 314.
[12] De Gennes, P. G., and Prost, J., 1993, *The Physics of Liquid Crystals* (Oxford: Oxford University Press).
[13] Madhusudana, N. V., 1994, *Phase Transitions*, **50,** 177.
[14] Kai, S., Andoh, M., and Yamaguchi, S., 1992, *Phys. Rev. A*, **46,** R7375.
[15] Alexe-Ionescu, A. L., Barbero, G., and Petrov, A. G., 1993, *Phys. Rev. E*, **48,** R1631.